Supporting Information

Mandl et al. 10.1073/pnas.1211717109

SI Materials and Methods

Mice. C57BL/6, splenectomised B6, Thy1.1$^+$ B6, and C57BL/10 mice were purchased from Jackson Laboratories. C57BL/10.A and CD45.1$^+$ H2-Aβ$^{-/-}$ (MHCII$^{-/-}$) B6 were purchased from Taconic Farms. β$_2$M$^{-/-}$ (MHCI$^{-/-}$) B6 were purchased either from Jackson Laboratories or from Taconic Farms. CD45.1$^+$ B6, K^{b}D$^{b-/-}$ (MHCI$^{-/-}$) B6, Lck-Cre B6, and CD45.1$^+$ B10.A were obtained from the National Institute of Allergy and Infectious Diseases contract colony at Taconic Farms.

Flow Cytometry. Anti-Thy1.1 (HIS51 or OX-7), CD4 (RM4-5), CD8 (53-6.7), CD45.1 (A20), CD45.2 (104), CD44 (IM7), CD5 (53-7.3), CD11a (2D7), chemokine (C-X-C motif) receptor 4 (CXCR4) (2B11), and P-selectin glycoprotein ligand-1 (PSGL-1) (2PH1) antibodies were purchased from eBioscience or BD Pharmingen. Anti-CCR7 (4B12) and CD29 (HMβ1-1) antibodies were purchased from BioLegend. UV-live/dead fixable dead cell stain kits were used according to the manufacturer's protocol. All samples were acquired on an LSRII flow cytometer (Becton Dickinson), and data were analyzed using FlowJo (Tree Star).

T-Cell Recirculation Block. To inhibit trafficking of T cells from blood into lymph nodes (LNs) and back into the blood, thus trapping T cells in either blood or LNs, splenectomized C57BL/6 mice were given 100 μg anti-αL and anti-α4 to block LN entry, in addition to 0.5 μg/g FTY720 i.p. to block LN egress, as previously described (1).

Transwell Migration Assays. To assess the fraction of cells capable of migrating toward a chemokine (C-C motif) ligand 21 (CCL21) or sphingosine-1-phosphate (S1P) gradient, 4×10^6 cells were added to 5-μm transwells (Corning Costar) whose bottom wells contained media alone, CCL21 (R&D Systems) or S1P (Cayman Chemical) and incubated for 3 h at 37 °C. For CCL21 migration assays, cells and chemokines were diluted in 5% (vol/vol) FCS-containing RPMI. For S1P migration assays, cells were rested for 30 min in serum-free RPMI at 37 °C and transwells incubated with 10% (vol/vol) FCS RPMI at 37 °C for 2 h, before washing the bottom wells with serum-free RPMI and adding cells to transwells. All wells were set up in duplicate. The percentage migrated cells was enumerated by running cells on a flow cytometer for a defined length of time and comparing acquired cell counts to premigration cell samples run in the same volume.

Dendritic Cell Cultures. WT and MHCII KO bone marrow-derived dendritic cells (DCs) were cultured in complete medium RPMI/10% (vol/vol) FCS with murine GM-CSF (5 ng/mL) and murine IL-4 (10 ng/mL) (Peprotech) as previously described (2). DCs were harvested and pulsed with LPS (10 ng/mL) at 37 °C for 1 h before fluorescent labeling and s.c. injection into recipient mice for imaging.

Two-Photon Imaging and Manual Analyses. After activating WT and MHCII KO DCs with LPS, DCs were differentially labeled with 25 μM Cell Tracker Blue, 5 μM Cell Tracker Orange, or 2.5 μM Carboxyfluorescein succinimidyl ester (CFSE) (all from Invitrogen), and an equal number (~1 × 10⁶ cells per mouse) of each population were mixed and injected s.c. into the right dorsal footpad of MHCII KO recipient mice. Eighteen to 48 h later, CD4$^+$ and CD8$^+$ T cells were isolated from B6 mice as described and labeled with either 5 μM SNARF-1 or 2.5 μM CFSE (Invitrogen). Equal numbers (~1 × 10⁷ cells per mouse) of each

cell type were then coinjected i.v. into the same recipients. Two to 24 h after T cell injection, recipient mice were anesthetized with nebulized isoflurane (2% induction, 1% maintenance) in 30% O2/70% air, with body temperatures maintained at 37 °C via a temperature-controlled environmental chamber and heating pads. The right popliteal LN was then surgically exposed and imaged through a 20× water immersion lens (N.A. 1.0) using a Leica SP5 on a DM6000 stage fitted with a 16W IR laser (Chameleon; Coherent) tuned to 800 nm. Imaging planes (760 × 760 μm) collected at 5-μm z-intervals were repeated at 15- to 30-s intervals for up to 2 h to yield xyzt data sets for processing and analysis by Imaris (BitPlane). The processed imaging series were converted to tiff series and subjected to either computational or manual analyses of contact frequency and duration. For manual analyses, individual DC–T-cell contacts were inspected using Imaris on xy images through z stacks. The number of sequential images in which a particular DC–T-cell contact was visually confirmed was multiplied by the fixed time interval between xyz imaging stacks to derive the duration of contact [contact duration = (frame number of continual DC:T-cell contact) × (time interval between xyz imaging frames)].

Automated Image Analyses. To be certain that there were no biases inadvertently introduced by our manual analysis of the imaging data, we also developed image analysis software to track the length of cell–cell interactions in an automated manner and used this software to analyze the same data sets. Image segmentation and analysis of imaging data were based on the image analysis software 2PISA that the authors developed previously (3) and that was extended by an automated cell-tracking feature. After the initial (static) interaction analysis was performed according to the protocol (3), the segmentation result was reprocessed using the novel cell-tracking module based on cell proximity and velocity information. This allows for a fully automated tracking of interacting pairs of cells and computation of dynamic interface properties and interaction statistics.

Modeling T-Cell Transit Dynamics. Because for both CD4$^+$ and CD8$^+$ T-cell populations the mean and SD of DC contact time were much smaller than mean transit time, a model of naïve T-cell transit through LN consistent with the exponential distribution of LN residence times is that T cells have a constant and small egress probability, q, after a DC encounter. In this model, a good approximation to the expected number of contacts, C, is simply $C = 1/q = 1/r\tau$, where r is the LN egress rate (h^{-1}) and τ is the mean DC contact time (h). In other words, $C =$ (mean transit time)/(mean duration of a single DC–T-cell contact). This is an upper bound on C because the calculation assumes that the time spent between DC is much smaller than the time spent in contact with DC. If this assumption does not hold, $C = 1/[r(\tau + \beta)]$, where β is the mean time spent moving from one DC to another.

We make the simplest (most parsimonious) assumption regarding egress, that the probability of a T cell leaving an LN after any given DC contact is a constant q, independent of the length of time that T cell has been resident in the LN, and independent of the total number of T cells in the LN. The probability of egress after exactly n contacts is then geometrically distributed as $q(1 - q)^{n-1}$, and the mean number of contacts a cell has while transiting is $1/q$. The mean number of contacts is large—on the order of hundreds (Fig. 5A)—and so q is much smaller than 1. In this case the number of contacts (n) is approximately exponentially distributed, with $P(n) \sim \exp(-nq)$. If interactions with DC

have mean duration τ, and the time between DC contacts is much smaller than τ, then the probability of a cell remaining in the lymph node a time T after entry is $P(T = nt) = P(n) \sim \exp(-Tq/\tau)$. (If cells spend a mean time β between DC contacts, τ is replaced with $\tau + \beta$). This model predicts exponentially distributed LN residence times, in agreement with our data, and $P(T) = \exp(-Tq/\tau)$, which is by definition: $\exp(-r\,T)$, where r is the egress rate. We measure both r and τ, so the probability of egress per DC interaction is $q = \tau.r$, or the mean contact duration (τ) divided by the mean transit time ($1/r$) (Fig. 5B).

It has been described that T cells reexpress surface S1PR1 to maximum levels only by 2–4 h after LN entry (4). The need to reacquire S1P sensitivity may impose a minimum LN dwell time. A more refined model of transit might divide populations into cells that are not yet competent to egress, and cells that egress with constant probability q per DC encounter. By using the simplest single-population model, we will slightly underestimate q and thus slightly overestimate the expected number of contacts each T cell makes with DCs. Our estimate of C is therefore an upper bound. However, even if the mean time of recently en-tered cells in which they are unable to egress is as long as 4 h, this does not substantially alter our conclusions.

Confocal Analysis of CD4$^+$ and CD8$^+$ T-Cell Localization. Total CD4$^+$ and CD8$^+$ T cells (~90% naïve, CD44^{lo}) were purified by negative selection using MACS (Miltenyi Biotec) and differentially dye labeled with 3 μM CellTracker Red (CMTPX) and 100 μM Cell-Tracker Blue (CMF$_2$HC), respectively, in PBS for 15 min at 37 °C. A total of 1.3×10^6 labeled CD4$^+$ and CD8$^+$ T cells were mixed 1:1 and injected i.v. into WT recipients. Inguinal LNs were harvested 24 h later, fixed, and stained as described with rabbit anti–LYVE-1 and rat anti–ERTR-7 (Novus Biologicals), then stained with anti-rabbit IgG Alexa Fluor 647 and anti-rat IgG Alexa Fluor 488 (Invitrogen) (5). Images were acquired using a Zeiss 710 confocal microscope with a motorized stage for tiled imaging.

Statistical Analyses. We analyzed data using GraphPad Prism or R Project version 2.10.1 (R Development Core Team, 2011). A criterion level of $P < 0.05$ (two-tailed) was used in all statistical analyses.

1. Matloubian M, et al. (2004) Lymphocyte egress from thymus and peripheral lymphoid organs is dependent on S1P receptor 1. *Nature* 427(6972):355–360.
2. Castellino F, et al. (2006) Chemokines enhance immunity by guiding naive CD8+ T cells to sites of CD4+ T cell-dendritic cell interaction. *Nature* 440(7086):890–895.
3. Klauschen F, Qi H, Egen JG, Germain RN, Meier-Schellersheim M (2009) Computational reconstruction of cell and tissue surfaces for modeling and data analysis. *Nat Protoc* 4 (7):1006–1012.
4. Lo CG, Xu Y, Proia RL, Cyster JG (2005) Cyclical modulation of sphingosine-1-phosphate receptor 1 surface expression during lymphocyte recirculation and relationship to lymphoid organ transit. *J Exp Med* 201(2):291–301.
5. Gerner MY, Kastenmuller W, Ifrim I, Kabat J, Germain RN (2012) Histo-cytometry: A method for highly multiplex quantitative tissue imaging analysis applied to dendritic cell subset microanatomy in lymph nodes. *Immunity* 37(2):364–376.
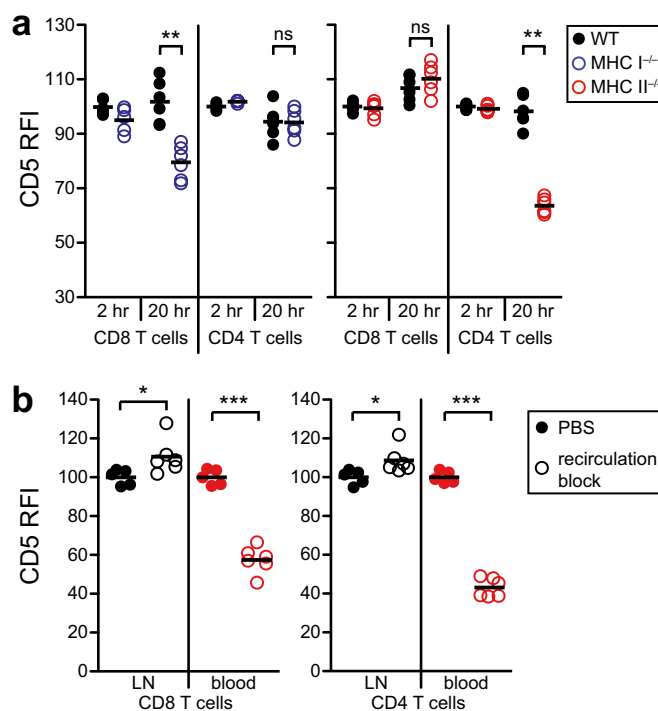
Fig. S1. Interactions of T cells with self-pMHC are ongoing and take place in secondary lymphoid organs. (A) Flow cytometric analysis of CD5 surface expression on CD4$^+$ and CD8$^+$ T cells in inguinal and brachial LNs 2 and 20 h after adoptive transfer into MHCI$^{-/-}$, MHCII$^{-/-}$, or WT recipients. RFI, relative fluorescent intensity, calculated as percentage of 0 h CD5 mean expression. (B) Expression of CD5 on CD4$^+$ and CD8$^+$ T cells in LNs or blood isolated from splenectomized mice 24 h after injection of PBS or anti-α4/αL and FTY720 to block both entry and egress from LNs. RFI calculated as percentage of CD4$^+$ or CD8$^+$ T cells in control group for LN or blood. ns, not significant; ***$P < 0.0001$; **$P < 0.005$; *$P < 0.05$. Data are pooled from two independent experiments each with three mice per group. Circles denote individual animals, lines represent means.
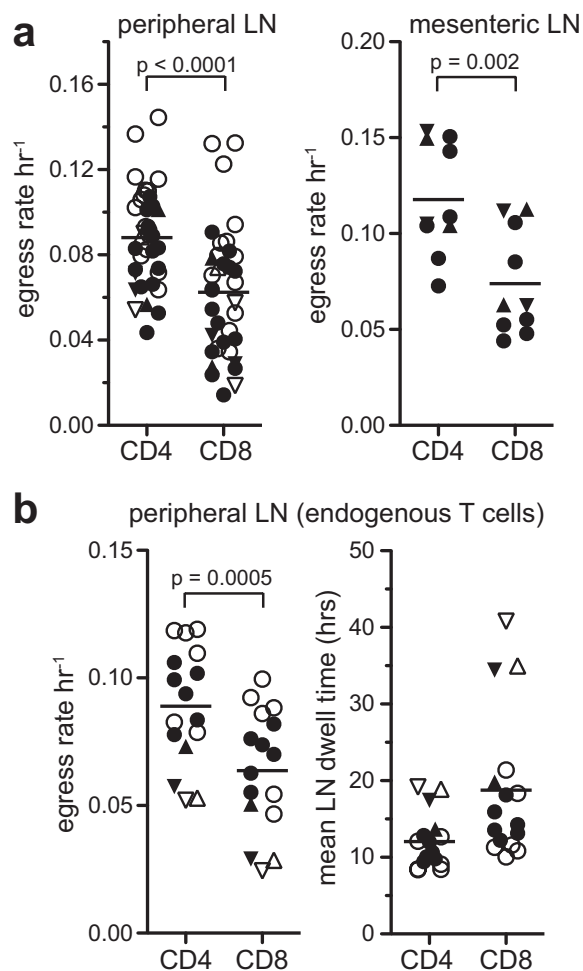
Fig. S2. CD4^{+} T cells have faster LN egress rates than CD8^{+} T cells. LN transit times of T cells were estimated after treatment of mice with integrin-blocking antibodies to prevent further entry of lymphocytes. (*A*) Egress rate estimates for transferred naïve CD4^{+} and CD8^{+} T cells in peripheral and mesenteric LNs. (*B*) Egress rate and mean dwell time estimates for endogenous naïve CD4^{+} and CD8^{+} T cells. Data points denote egress estimates from one experiment (as shown in Fig. 2*C*). Lines represent calculated means. Closed symbols, iLN; open symbols, bLN; ●, B6 mice; ▲, B10.A mice; ▼, B10 mice; egress estimates were obtained from 8 to 19 independent experiments.

Fig. S3. Similar CD4+ and CD8+ T-cell localization and dynamic behavior in the LN. (*A*) A total of 1.3×10^6 CMTPX-labeled CD4+ T cel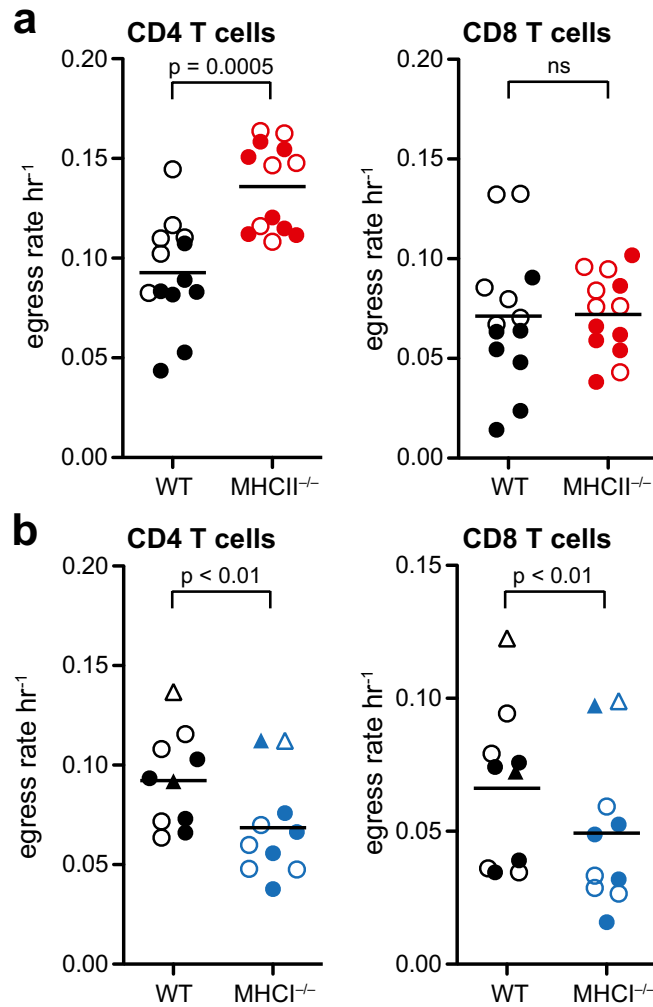ls and CMF$_2$HC-labeled CD8+ T cells were transferred i.v. into WT recipients. Twenty-four hours later, an inguinal LN was harvested, fixed, cut into 20-μm sections, and stained with ERTR-7 and LYVE-1. (*Right*) Image is magnified from boxed region at *Left*. (*B*) A total of 4×10^6 CMFDA+ CD8+ T cells and CMTPX+ CD4+ T cells were transferred and the inguinal LN imaged using two-proton (2P) intravital microscopy 18 h later. (*Left*) Snapshot of T cells moving (Movie S2); (*Right*) Individual CD4+ and CD8+ T-cell tracks during a period of 44 min. (Scale bar, 40 μm.) (*C*) Quantification of mean and maximum velocity, fraction of cells arrested, and total displacement for CD4+ and CD8+ T cells. Circles represent means calculated from one 2P microscopy movie. Data are shown from nine independent movies. (*D*) Responsiveness of naïve CD4+ and CD8+ T cells to indicated concentrations of S1P (in nM) as assessed by transwell migration assays. A representative example from one mouse is shown (assays were performed in duplicate).

Fig. S4. Expression of LN homing and adhesion receptors on naïve CD4$^+$ and CD8$^+$ T cells. (*A*) Surface expression of CD11a, CXCR4, CD29, PSGL-1, and CD62L on naïve CD4+ and CD8+ T cells. Example fluorescent intensity histograms from representative mice are shown. (*B*) CCR7 surface expression on a cohort of adoptively transferred naïve CD4$^+$ and CD8$^+$ T cells at different time points after anti-α4/αL administration to block LN entry measured in the inguinal LN. (*Left*) Geometric mean fluorescent intensity (MFI); (*Right*) Relative fluorescent intensity (RFI) normalized to the mean level in transferred CD4$^+$ and CD8$^+$ T cells at 0 h. Data are from four to six mice per time point.

Fig. S5. Faster LN egress rates of CD4+ T cells in the absence of MHCII but not of CD8+ T cells in the absence of MHCI. LN egress rate estimates for transferred naïve CD4+ and CD8+ T cells in WT and MHCII−/− (a), or WT and MHCI−/− (b). Circles denote transit time estimates from one experiment. Lines represent group means obtained from five to seven independent experiments. Closed symbols, iLN; open symbols, bLN. In (b): ●, β2M−/−- or WT-matched recipients; ▲, KᵇDᵇ−/−- or WT-matched recipients.
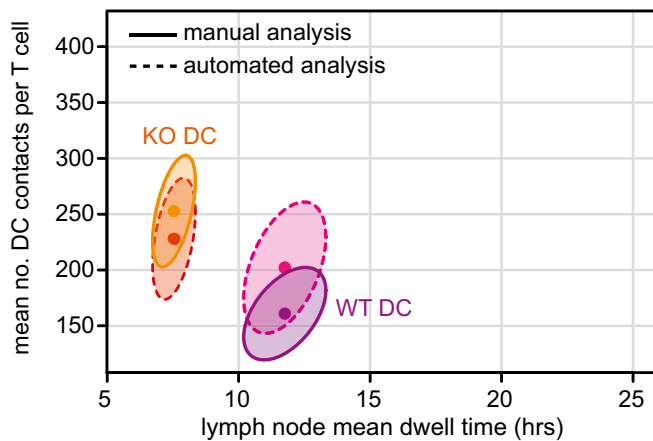

Fig. S6. DC scanning dynamics of CD4+ T cells in LNs is altered when DCs do not express MHCII. Estimates of the mean number of WT or MHCII KO DCs scanned by an individual CD4+ T cell during steady-state LN transit. Means (points) with bootstrapped joint 95% confidence intervals (shaded areas) are shown for DC–T-cell contacts obtained from both the manual and automated estimates of the distributions of DC contact times.
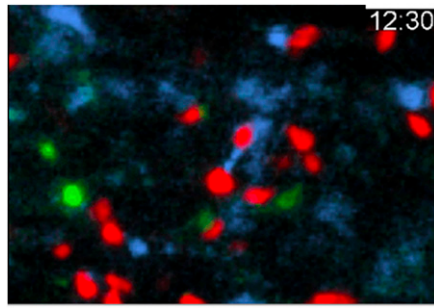
Movie S1.   Contacts between CD4$^+$ T cells and MHCII$^{+/+}$ or MHCII$^{-/-}$ DCs in the lymph node in the absence of antigen. CD4$^+$ T cells (red) interacting with WT (blue) or MHCII$^{-/-}$ (green) DCs in vivo. (Scale bar, 20 μm.) Time is shown in min:s.

[Movie S1](#)
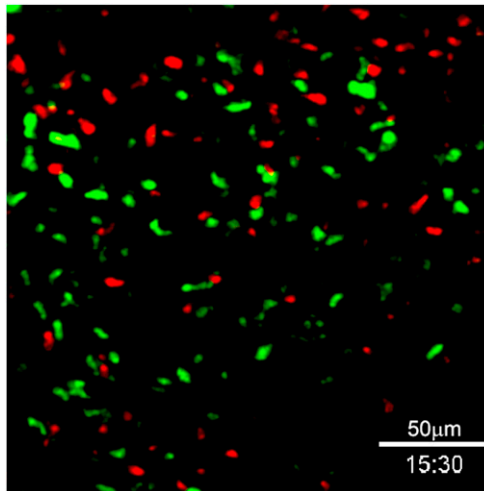
Movie S2.   Dynamic behavior of naïve CD4$^+$ and CD8$^+$ T cells in the lymph node. CD4$^+$ T cells (red) and CD8$^+$ T cells (green) in the inguinal LN (from Fig. S2*B*). (Scale bar, 50 μm.) Time is shown in min:s.

[Movie S2](#)